Simulated solvation of organic ions II: Study of linear alkylated

Céline Houriez, Meot-Ner Michael, Michel Masella

Simulated solvation of organic ions II: Study of linear alkylated carboxylate ions in water nanodrops and in liquid water. Propensity for air/water interface and convergence to bulk solvation properties

Céline Houriez,[1] Michael Meot-Ner (Mautner),[2] and Michel Masella[3]

[1]*MINES ParisTech, PSL Research University,*
CTP - Centre Thermodynamique des Procédés,
35 rue Saint-Honoré, 77300 Fontainebleau, France
[2]*Department of Chemistry, Virginia Commonwealth University, Richmond,*
Virginia 23284-2006, United States, and Department of Chemistry,
University of Canterbury, Christchurch, New Zealand 8001
[3]*Laboratoire de Biologie Structurale et Radiobiologie,*
Service de Bioénergétique, Biologie Structurale et Mécanismes,
Institut de Biologie et de Technologies de Saclay,
CEA Saclay, F-91191 Gif sur Yvette Cedex, France

Abstract

We investigated the behavior of six linear alkylated carboxylate ions, from methanoate (formate) to hexanoate, in small water droplets comprising from 50 to 1000 water molecules or in neat water, by a computational protocol based on standard molecular dynamics schemes and on sophisticated polarizable models to handle both ion/water and water/water interactions. Our results show that in small droplets all of the alkylated carboxylate ions from methanoate to hexanoate present a strong propensity for the air/water interface. This propensity is lowered as the droplet size increases, so that only carboxylate ions larger than propanoate still have a noticeable propensity for the interface, in agreement with recent experimental findings. For these larger ions, transfer to the surface reduces enthalpic stabilization by ion/water dispersion effects in the interior by 3 kcal mol^{-1} per methylene (CH_2) group, similar to hydrophobic solvation effects from cluster-based analysis. However, this is compensated by entropy effects of $> +3.3$ cal mol^{-1} K^{-1} per CH_2 group. These effects in the model reproduce the known structure-making effects of the alkyl groups in solution, and their loss upon transfer to the surface. There the carboxylate ion headgroups are strongly oriented near the air/water interface with the anionic head pointing towards the aqueous core, while the hydrophobic alkyl chains are repelled into air and desolvate, losing their structure-making effects. Further, comparison with alkylammonium ions shows that the hydrocarbon chains of anions and cations solvate similarly, and the ionic headgroups and alkyl substituents solvate as independent solutes. From droplet data, we estimated the carboxylate single absolute solvation enthalpies using standard extrapolation schemes. For the two smallest carboxylate ions, the results yield an absolute proton solvation enthalpy close to the experiment-based value, similar to the value reported in our former study dealing with methylated ammonium ions (about 270 kcal mol^{-1}). However, the extrapolated proton solvation enthalpy for the largest carboxylate ions is smaller by about 10 kcal mol^{-1}. The origin of this discrepancy will have to be investigated by much larger droplets whose simulations are still demanding.

Keywords. Organic ion solvation, carboxylate ions, molecular dynamics, droplets, hydrophobic solvation, air/water interfaces.

I. INTRODUCTION

Ion behavior at aqueous interfaces is a major research field in physics, chemistry and biology. In particular, it drives many important atmospheric and environmental chemistry processes [2, 3]. It plays also a key role in understanding acid-base reactions at air/water interfaces that govern many important processes in the living cell, from enzyme catalysis to molecular recognition, and in understanding surfactants and self-assembly to form membranes, micelles and vesicles [4–7].

When considering organic ions, many of them contain both hydrophobic and hydrophilic moieties that modulate their hydration properties, as well as their behavior at air/water interfaces. Among these ions, alkylcarboxylate ions are of particular interest because (1) they are among the simplest ionic systems presenting both a hydrophilic anionic head and a hydrophobic alkyl side chain and (2) they are a major component of many biological macromolecules (from proteins to cell membranes). We may also quote that these ions were shown to contribute significantly to the cloud droplet forming ability [8]. However, even for simple carboxylate ions solvated in bulk water, most of the experimental data reported to date focus on the hydration properties of their COO^- head [9–12], and only sparse data were reported concerning the effects of their hydrophobic moiety on their solvation process. This is in part due to similarity of the time scale of the water dynamics in the bulk and in the vicinity of small solutes (see among others the discussions provided in Refs. 13 and 14). Nevertheless, by analyzing surface sensitive core-level electron spectra, Ottosson and coworkers [15] concluded recently that the propensity of alkylcarboxylate ions for the air/liquid water interface increases when lengthening their alkyl side chain and that only large enough alkylcarboxylate ions, starting at butanoate, have a noticeable propensity for this interface.

An alternative route to investigate the behavior of ions in aqueous media and at interfaces is to consider computer simulations at the microscopic level. For instance, several studies concerning the behavior of carboxylate ions both in neat water and at the air/liquid water interface have been reported. To perform reliable simulations of organic ions, accurate computational protocols able to simulate both water/water and ion/water interactions are needed. However, the most sophisticated protocols, based for instance on DFT molecular dynamics or on hybrid QM/MM approaches, are highly computationally demanding.

That explains why they were used to investigate only the smallest carboxylate ions, namely $HCOO^-$ and CH_3COO^-, solvated in liquid water [16–18]. Only a few studies were devoted to theoretically investigate complex aqueous solutions involving carboxylate ions or the behavior of carboxylate ions at the air/liquid water interface. Most of them were based on efficient but simple pairwise forcefields [19–23], and we may quote only a few attempts to use sophisticated polarizable approaches to investigate the hydration of the COO^- moiety, as in simple organic ions [24], in the glycine zwitterion and in the aspartylalanine dipeptide [25]. However, many authors [26–30] pronounced it necessary to explicitly considering microscopic polarization effects in simulating the propensity of polarizable ions, like carboxylates, for the air/water interface. Moreover, all the standard pairwise water forcefields used up to now to simulate organic ions in bulk water are known for their poor ability to describe water aggregates in gas phase (cf. the discussions in Ref. [31], for instance). Hence, simulating carboxylate hydration process by sophisticated and accurate polarizable models may provide new and useful data for interpreting experiments. That will help also to assess the ability of commonly used standard pairwise forcefields to model the hydration of single or multiple ions not only in the bulk phase but also in droplets [32].

The aim of the present work is to investigate the behavior of six small linear alkylated carboxylate ions, from methanoate to hexanoate, in small water droplets, comprising from 50 to 1000 water molecules, and in neat water. To this end, we use sophisticated polarizable models to handle both ion/water and water/water interactions, namely the water rigid model TCPE/2013 [33] and a COO^-/water model similar to the recent one proposed to model halide hydration [34]. These two approaches were shown to accurately model pure water and halide/water systems in the gas phase as well as in the bulk. We use the same computational protocol based on standard molecular dynamics schemes as in our recent study dealing with the solvation of methylated ammonium ions in water nanodroplets [35]. The present study focuses mainly on evaluating the effects both of the alkyl side chain length and of the droplet size on the propensity of carboxylate ions for the air/water interface. Here, we investigate only the solvation of a single carboxylate anion in a pure water environment without considering any acid association/dissociation phenomena at the air/water interface, for which many conflicting results have been reported (see the recent discussions in Ref. [36]). Note that our simulation protocol will yield equilibrium thermochemistry values (like ion/water and water/water interaction enthalpies) which are independent of other equilibria

that the species participate in. Among the ion solvation properties, we mainly focus our analyses on the possible change in the carboxylate structure and orientation when crossing the air/water interface, and on the single carboxylate ion absolute solvation enthalpies estimated from droplet data, by using four different extrapolation schemes based on power-law functions of the droplet size. Previously, we considered only one fitting function in our study about methylated ammonium ions. For the sake of comparison, we thus extrapolate here again the solvation enthalpies of these cations using the four extrapolation schemes to further discuss their ability in providing reliable results.

II. THEORETICAL METHODS

In the following, N is the total number of atoms considered, M is the total number of atoms in an ion, N_μ is the total number of polarizable atoms, N_w is the total number of water molecules and M_w is the total number of atoms belonging to the water molecules. All molecular modeling computations were performed with our own code POLARIS(MD) as in our former study regarding ammonium ions [35]. All quantum computations were performed by means of the GAUSSIAN09 package of programs [37], using the frozen core approximation systematically.

A. The model

The total potential energy U of a carboxylate/water system, *i.e.* the energy of the reaction $n\mathrm{H_2O}$ + carboxylate $\rightarrow$ carboxylate/$(\mathrm{H_2O})_n$, is decomposed into three terms: the ion internal energy U^{rel}, and the ion/water U^{iw} and water/water U^{ww} interaction energies.

As in our former study concerning ammonium ions [35], we consider here the rigid water model TCPE/2013 [33]. Besides the repulsive and Coulombic energy terms (U^{rep} and $U^{qq'}$), TCPE/2013 also includes a polarization energy term U^{pol} (based on an induced point dipole moment approach) and a short-range anisotropic many-body energy term U^{hb} to accurately reproduce hydrogen bond (HB) network properties. Analytically, the term U^{hb} is close to U^{shb} used to model carboxylate/water interactions (see below). The sum of the four terms,

$$U^{ww} = U^{rep} + U^{qq'} + U^{pol} + U^{hb}, \tag{1}$$

gives the total potential energy of a pure molecular water system, with respect to individual unbound gas phase molecules. TCPE/2013 is shown to model accurately liquid water over a wide range of thermodynamic conditions, as well as water clusters in gas phase and the water interactions in cation first hydration shells [33]. For systems composed of anions like Br^- and I^- interacting directly with 4 to 8 water molecules, TCPE/2013 is also shown to reproduce high level quantum computation results concerning the water interaction energies, within 1 kcal mol^{-1} on average [38].

The carboxylate/water energy term U^{iw} is the sum of six terms:

$$U^{iw} = U^{rep} + U^{qq'} + U^{pol} + U^{disp} + U^{shb} + U^{rel}. \tag{2}$$

The repulsive U^{rep}, Coulombic $U^{qq'}$, and dispersion U^{disp} terms are defined as

$$U^{rep} = \sum_{i=1}^{M} \sum_{j=1}^{M_w} a_{ij} \exp\left(-b_{ij} r_{ij}\right), \tag{3}$$

$$U^{qq'} = \sum_{i=1}^{M} \sum_{j=1}^{M_w} \frac{q_i q_j}{4\pi\epsilon_0 r_{ij}}, \tag{4}$$

$$U^{disp} = -\sum_{i=1}^{M} \sum_{j=1}^{M_w} \left(\frac{r^*_{ij}}{r_{ij}}\right)^6. \tag{5}$$

Here, r_{ij} is the distance between the atoms i and j, q_i are the static charges located on atomic centers, and a_{ij}, b_{ij} and r^*_{ij} are adjustable parameters. The repulsive term U^{rep} is truncated for distances larger than 5.0 Å. Dispersion effects are accounted for by considering only interactions between water oxygen atoms and carbon atoms. The energy term U^{rel} is introduced to handle the intramolecular degrees of freedom of the carboxylate ion. It includes standard stretching, bending and torsional terms, as well as an improper torsional term $U^{imp} = \frac{1}{2} k_{imp} \psi^2$, where ψ is the improper dihedral angle $\angle OC_1C_2O$ (see Figure 1 for labelling).

The polarisation energy term U^{pol} including both ion/water and water/water interactions is defined as

$$U^{pol} = \frac{1}{2} \sum_{i=1}^{N_\mu} \frac{p_i^2}{\alpha_i} - \sum_{i=1}^{N_\mu} \boldsymbol{p}_i \cdot \mathbf{E}_i^q - \frac{1}{2} \sum_{i=1}^{N_\mu} \sum_{j=1}^{N^*_\mu} \boldsymbol{p}_i \mathbf{T}_{ij} \boldsymbol{p}_j. \tag{6}$$

Here, the superscript * indicates that the corresponding sum includes only pairs of atoms separated by more than two chemical bonds. Only non-hydrogen atoms are considered as

polarizable centers, with an isotropic polarizability α_i and an induced dipole moment $\boldsymbol{p}_i$ given by

$$\boldsymbol{p}_i = \alpha_i \cdot \left(\mathbf{E}_i^q + \sum_{j=1}^{N_\mu^*} \mathbf{T}_{ij} \cdot \boldsymbol{p}_j \right). \tag{7}$$

$\mathbf{T}_{ij}$ is the dipolar interaction tensor and $\mathbf{E}_i^q$ is the electric field generated on the polarizable center i by the surrounding static charges q_j. $\mathbf{T}_{ij}$ and $\mathbf{E}_i^q$ both include an intermolecular short-range damping component, corresponding to a radial charge distribution $\rho(r) \propto \exp(-c \times r^3)$, with c a parameter and r the distance from an atomic center [39].

Lastly, we consider also the many-body anisotropic short-range energy term U^{shb}, which was recently proposed to model halide/water interactions [33]:

$$U^{shb} = \sum f(r)g(\psi). \tag{8}$$

The sum runs over all the carboxylate/water strong hydrogen bonds (SHB). f and g are Gaussian functions:

$$f(r) = D_e \exp\left[-\frac{(r_{shb} - r_{e,shb})^2}{\gamma_r} \right] \quad \text{and} \quad g(\psi) = \exp\left[-\frac{(\psi - \psi_e)^2}{\gamma_\psi} \right]. \tag{9}$$

r_{shb} is the SHB length and ψ is the $\mathrm{O-H\cdots O_{carboxylate}}$ angle. $r_{e,shb}$ and ψ_e are their equilibrium values. To account for the chemical environment effect on the strength of a local SHB, D_e is taken as a linear function of the local density of water O-H bonds, ρ_{oh}, in the anion vicinity: $D_e = d_e(1 - \xi\rho_{oh})$, with d_e and ξ two adjustable parameters. ρ_{oh} is estimated according to

$$\rho_{oh} = \sum \exp\left[-\frac{(r_{shb} - r_{e,shb})^2}{\gamma'_{rt}} \right]. \tag{10}$$

Here, the sum runs over all the water/carboxylate SHB, apart from the local one considered explicitly in the present function f. γ'_{rt} is a parameter adjusted to take into account mainly the water molecules of the first hydration shell of the COO^- moiety (here, γ'_{rt} is set to 0.3 Å). U^{shb} is smoothly zeroed between r_{shb} distances of 5.5 and 6.0 Å, using a fifth order spline function.

Originally, U^{shb} was used to account for the charge transfer effects occurring in halide/water SHB [34]. In the present study, it is introduced to destabilize a particular $CH_3COO^-/(H_2O)_2$ trimer structure, labelled **2-0** in Figure 1. MP2/aug-cc-pVTZ quantum computations show this structure to be unstable, since it evolves towards the structure **2-1** during the geometry optimization process. By considering only the five other energy terms of U^{iw}, we were not

able to destabilize this particular structure **2-0** while this can be readily done by using the U^{shb} term with an anti-cooperative parameter $\xi < 0$. We may note here that the formation of anti-cooperative SHBs between the carboxylate moiety and water molecules was recently invoked to interpret experimental infrared spectroscopy data concerning the carboxylate group hydration [9].

To assign the U^{iw} parameters, we consider as reference data the quantum results concerning eight small $CH_3COO^-/(H_2O)_n$ clusters (n=1-4). Their geometries were optimized at the MP2/aug-cc-pVTZ level. The cluster binding energies (BE_n) were estimated at the complete basis set (CBS) limit, according to the same computational protocol as in Ref. 35. To assign the charges of the COO^- moiety, we consider the quantum Natural Population Analysis results concerning the isolated ion CH_3COO^-, and the charges of the side chain methylene groups were assigned according to the same protocol as in our former study dealing with methylated ammonium ions [35]. The isotropic atomic polarizabilities for the carboxylate oxygen and carbon atoms were assigned to reproduce the molecular polarizability of CH_3COO^- computed at the MP2/aug-cc-pVQZ level (4.9 Å^3), and knowing our earlier value for methyl carbon (2.1 Å^3). We assume here that the polarizabilities of the COO^- moiety atoms are close to each other. Lastly, from our computations, it appears that the polarization damping effects don't play a pivotal role to reproduce accurately the quantum BE_n. The damping parameters c are thus chosen to make the carboxylate/water damping effects small (i.e. $c = 0.3$ Å^{-3}).

The torsional parameters corresponding to all the carboxylate dihedral angles, like ∠OCCH or ∠CCCC, were assigned to reproduce at best the quantum energy profiles of these angles computed at the MP2/aug-cc-pVTZ level, and by considering all the other model parameters defined as above. In particular, these torsional parameters allow one to reproduce the differences in energy among the different minima of the dihedral angle energy profiles. Lastly, all the other parameters of U^{rel} are taken from the CHARMM 2.7 forcefield [40].

Most of the above-mentioned quantum results, the carboxylate/water cluster structures and the U^{iw} parameter set are provided as Supporting Information. The optimum parameter set allows one to reproduce the cluster SHB lengths within less than 0.05 Å on average and the quantum CBS BE_n within less than 0.75 kcal mol^{-1} on average (the BE_n range from 20 to 67 kcal mol^{-1} for n=1-4).

B. Simulation details

MD simulations of carboxylate/water droplet systems and of carboxylate molecules at the air/liquid water interface are performed in the NVT ensemble. Bulk carboxylate/water systems are simulated in the NPT ensemble. Bulk and air/liquid water interface systems include about 1000 and 2000 water molecules, respectively. The simulation duration is 10 ns and all the trajectories are sampled each 1 ps. The potentials of mean force (PMF) corresponding to the interaction of a carboxylate ion with a water system (droplet or liquid water) are computed according to a standard umbrella sampling protocol. The degree of freedom constrained during these simulations, d, is either the distance between the carbon atom of the COO^- moiety and the droplet center of mass (COM), or the projection of the distance between the carboxylate carbon and the simulation cell center (SCC) on the axis orthogonal to the air/liquid water interface . The details of these protocols are provided as Supporting Information. The target value of the d along an umbrella sampling simulation is denoted d_c.

While no truncation is applied to the different energy terms in droplet simulations (with the exception of U^{rep} and U^{shb}), ion/water dispersion interactions are truncated in simulations of the bulk phase and of the air/liquid water interface for distances larger than $R_{\text{cutoff}} = 12$ Å (corresponding to the cutoff value for the Ewald direct energy terms used to simulate liquid water systems). Hence, for comparison purposes with droplet results, the PMF computed from bulk simulations have to be corrected to account for the dispersion truncation. For the present discussions, we only apply such a correction to the PMF minimum values observed close to the air/liquid water interface (see below), by adding the following amount of energy to the PMF values:

$$\delta\text{PMF} = \int_{R_{\text{cutoff}}}^{\infty} -\sum \left(\frac{r_{ij}^*}{r}\right)^6 \times 4\pi r^2 \rho_s dr = \frac{4\pi\rho_s}{3R_{\text{cutoff}}^3} \times \sum (r_{ij}^*)^6. \tag{11}$$

The sum runs over all the carboxylate dispersion centers and ρ_s is the solvent density (taken as a constant and equal to the water bulk density, 0.0331 molecule $Å^{-1}$). This represents the upper limit of the amount of energy not accounted for in bulk simulations when using a cutoff to handle ion/water dispersion. The magnitude of δPMF ranges from 0.11 ($HCOO^-$) to 0.39 kcal mol^{-1} ($C_5H_{11}COO^-$).

To minimize the impact of evaporation phenomena in the droplet simulations, we used

the same computational protocol as in our ammonium study [35]. Droplet systems are confined in a spherical cavity, whose radius corresponds to the largest droplet COM/water oxygen distance to which 12 Å are added. As a water molecule crosses the cavity boundary, it undergoes a reflexion from a perfect elastic collision with the cavity wall. With such a protocol, we showed that the total number of interacting water molecules in a droplet differs on average by 0.3 molecules from the total number of water molecules N_w along the 10 ns ion/droplet simulations, leading to an uncertainty affecting the water/water interaction energy of 5 kcal mol^{-1} at most [35].

III. RESULTS AND DISCUSSION

A. Carboxylate molecules in gas and liquid phases

1. Carboxylate structures in gas phase

Here, we discuss the most stable carboxylate structures in gas phase, in terms of dihedral angles $\angle C_nC_{n+1}C_{n+2}C_{n+3}$, whose values are denoted by Ψ_{n+3} (see Figure 1). The most stable carboxylate conformations were identified by performing 1 ns simulations in gas phase at a constant temperature of 300 K, and by systematically quenching the trajectories each 1 ps.

For the hexanoate, the most stable structure predicted by our model is shown in Figure 1. The Ψ_{n+3} values are 67, 50 and 178° for $n = 1 - 3$, respectively. The Ψ_{n+3} values given by our model for the most stable butanoate and pentanoate structures are in line with the hexanoate ones. For instance, in the case of the butanoate, the angles Ψ_4 and Ψ_5 are of 69 and 60°, respectively. Hence, our model predicts the dihedral angles close to the carboxylate anionic head to be in a gauche conformation, while a dihedral anti conformation is observed for methyl groups distant by more than 3 carbon atoms from the COO^- moiety. This result agrees with our quantum computations concerning the propanoate and the butanoate (see the dihedral energy profiles provided as Supporting Information). Note that the Ψ_{n+3} values are 52, 57 and 177° in the optimized structure of pentanoate, obtained from MP2/aug-cc-pVDZ quantum computations, and by considering as starting point the most stable structure given by our model. From the crystallographic structures of the Cambridge Structural Database (CSD) [41], a gauche conformation for the dihedral angle Ψ_4 is observed in 30% of the CSD structures for both pentanoate and hexanoate and between 30% (pentanoate) and

15% (hexanoate) for Ψ_5. For the hexanoate Ψ_6 angle, less than 10% of the CSD structures are in a gauche conformation. Keeping in mind the constraints occuring in the solid phase, our model data are in a reasonable agreement with the CSD ones for the latter dihedral angles.

Lastly, for the forthcoming discussions of Section III C, the distances between the carbon atoms of the COO^- and CH_3 moieties in the most stable gas phase carboxylate structures are 1.5, 3.3, 3.9 and 4.9 Å from ethanoate to hexanoate, respectively.

2. Solvent structure in the vicinity of carboxylate ions in liquid water

To assess the reliability of our model to simulate the hydration process of carboxylate ions in large water systems, we discuss here the water structure in the vicinity of the COO^- moiety in the liquid phase, observed along the NPT bulk simulations. Moreover, we compare our results to earlier data computed from QM/MM hybrid and Car-Parrinello simulations [16–18], as well as to experiments [9–12].

Figure 2 shows the radial distribution functions computed along the bulk simulations, and corresponding to COO^- oxygen/water oxygen [$g_{OO_w}(r)$], COO^- carbon/water oxygen [$g_{CO_w}(r)$], and COO^- oxygen/water hydrogen [$g_{OH_w}(r)$]. The first peak positions of our three kinds of distribution functions are located around 2.70, 3.60 and 1.70 ± 0.05 Å, regardless of the carboxylate ion. For the alkylated carboxylate ions, the first minima of the distribution functions are located around 3.50, 4.10 and 2.45 ± 0.05 Å for $g_{OO_w}(r)$, $g_{CO_w}(r)$ and $g_{OH_w}(r)$, and the coordination numbers are 3.1 ± 0.1 and 3.2 ± 0.1, and 7.8 ± 0.2 for the two oxygen atoms and the carbon atom of the COO^- moiety, respectively. Regarding the functions $g_{OO_w}(r)$ and $g_{OH_w}(r)$, the profiles of their first peak are similar for all the carboxylate ions. This result was expected, as the first peaks correspond to the direct interactions of water molecules with the COO^- moiety, which are slightly influenced by the carboxylate aliphatic chain.

The main features of all these distribution functions are in line with those derived from QM/MM simulations with several DFT levels of theory concerning $HCOO^-$ and CH_3COO^- in neat water [17, 18]. For instance, for $HCOO^-$, the positions of the first peaks were found to be 2.67–2.76 Å for $g_{OO_w}(r)$ and 1.71–1.84 Å for $g_{OH_w}(r)$ [17]. For CH_3COO^-, the first peaks are located around 2.66–2.74 Å for $g_{OO_w}(r)$, 3.50–3.60 Å for $g_{CO_w}(r)$, and 1.67–1.78

Å for $g_{\mathrm{OH_w}}(r)$, and the corresponding coordination numbers are 2.9–3.0 per COO^- oxygen, and 7.6–8.3 for the COO^- carbon [18]. Our results are also in very good agreement with those obtained from classical MD and Monte Carlo simulations with pairwise or polarizable forcefields [19, 20, 24]. In all of these studies, the first peaks of the radial distribution functions are located around 2.7, 3.7, and 1.7 Å for $g_{\mathrm{OO_w}}(r)$, $g_{\mathrm{CO_w}}(r)$, and $g_{\mathrm{OH_w}}(r)$, respectively. The coordination numbers per carboxylate oxygen are found to be 3.6 in the case of $HCOO^-$ [20] and around 3.4 for CH_3COO^- [19, 20, 24].

For the $g_{\mathrm{OO_w}}(r)$ second peak, its height decreases as we lengthen the carboxylate side chain. This result originates from the side chain steric effect that prevents water molecules to interact in the direction of the carboxylate $OOC - R$ axis (R = H, C). Hence, more water molecules are allowed to interact at short range with the COO^- carbon for the smallest carboxylate ions than for the larger ones. That also explains the different properties of the function $g_{\mathrm{CO_w}}(r)$ for $HCOO^-$, relative to alkylated carboxylates. For instance, in the case of $HCOO^-$, the height of the $g_{\mathrm{CO_w}}(r)$ first peak is 2.8 and the first minimum is around 4.5 Å while the corresponding values for alkylated ions are about 2.3 and 4.1 Å. That yields a coordination number for the $HCOO^-$ carbon atom almost twice larger than for the alkylated carboxylate ions, respectively 13.5 and 7.8.

Experimentally, the hydration number per COO^- oxygen ranges from 1.2 to 4.5 (see among others Refs. 13, 14, and 42 and the references cited therein). Such a large range of values originates from both the different experimental conditions used and the different definitions considered for the hydration number, preventing a direct comparison with theoretical estimates. Nevertheless, our computed hydration numbers for the COO^- oxygen atoms agree with the most accepted experimental values, ranging from 2.5 to 3.0.

3. Bulk water destabilization and ion deformation energies

Besides the ion/water interaction energies, two other important quantities have to be taken into account to investigate the energetics of the ionic solvation process: the bulk water destabilization energies $\Delta\bar{U}^{ww}_{\mathrm{bulk}}$ due to the ion presence and the intramolecular deformation energies $\Delta\bar{U}^{\mathrm{ion}}_{\mathrm{intra}}$ between gas phase and solution for polyatomic ions.

We estimated the water destabilization energies by comparing the water/water interaction energies from simulations of neat water and of an hydrated ion. The ion intramolecular

deformation energies were computed from the sets of ion coordinates extracted from bulk simulations. The corresponding averaged energies are then subtracted from the isolated ion energies at T = 300 K, computed from 1 ns gas phase simulations. $\Delta\bar{U}^{ww}_{\rm bulk}$ and $\Delta\bar{U}^{\rm ion}_{\rm intra}$ are summarized in Table II for the carboxylates and for the methylated ammonium ions and K^+, as computed from the data of our former study [35]. Concerning the latter cations, the water destabilization energies $\Delta\bar{U}^{ww}_{\rm bulk}$ were computed in our previous study from simulations performed using classical Ewald summation techniques for neat water and the Particle Mesh Ewald method for ionic solutions. The values reported here correspond to data computed using the same Particle Mesh Ewald protocol. That explains the weak differences in values of Table II for the cations, relative to the original values [35].

The deformation energies $\Delta\bar{U}^{\rm ion}_{\rm intra}$ are small for all the ions. They are at most of about 1 kcal $\rm mol^{-1}$ for the largest carboxylates while they are all negligible for the cations and the smallest carboxylates (< 0.3 kcal $\rm mol^{-1}$). Similar to the methylated ammonium ions [35], the water destabilization energies $\Delta\bar{U}^{ww}_{\rm bulk}$ are very similar for all the carboxylates (around 47.0 ± 0.7 kcal $\rm mol^{-1}$). This result will be further discussed below.

B. Probability of ion location and ion/water PMF at air/water interfaces

The ion/water PMF relates to the ion/water system partition function Z

$$Z \propto \int \exp\left[-\mathrm{PMF}(d)/k_B\mathrm{T}\right] dv. \tag{12}$$

Here, d corresponds either to the distance r between the carbon atom of the COO^- moiety and the droplet COM, or to the projection z of the distance between this carbon atom and the cell center on the axis orthogonal to the interface, when simulating air/liquid water interfaces. As in the case of the ammonium/water droplets, the carboxylate ions interact with quasi-spherical droplets, regardless of the droplet size and of the carboxylate. Hence, $dv \propto r^2 dr$ for ion/water droplet systems and $dv \propto dz$ for air/liquid water systems.

For air/liquid water systems, the probability density of finding an ion at a position z is

$$P(z) = \exp\left[-\mathrm{PMF}(z)/k_B\mathrm{T}\right]/Z. \tag{13}$$

By considering the entropic term $\mathrm{TS}_{geom}(r) = k_B\mathrm{T}\ln(r^2)$, the probability density $P(r)$ of finding an ion at a distance r from the droplet COM is

$$P(r) = \exp\left\{-[\mathrm{PMF}(r) - \mathrm{TS}_{geom}(r)]/k_B\mathrm{T}\right\}/Z. \tag{14}$$

The PMF for carboxylate/droplet systems are shown in Figure 3. The corresponding density probabilities $P(r)$ and the air/liquid water PMFs are provided as Supporting Information. The entropic term $\mathrm{TS}_{geom}(r)$ represents the larger accessible volume as the distance r increases for a quasi spherical droplet. It plays a noticeable role when $\mathrm{PMF}(r)$ is flat enough, as for the present carboxylate ions, *i.e.* it drives the ions towards the interface. For instance, in the case of $N_w = 1000$ droplet systems, by estimating the mean distance r from probability densities computed by accounting for it or not (these densities are both provided as Supporting Information), we show that this entropic term is responsible for an increase of the mean distance r by about 3-4 Å for carboxylates with a strong interface propensity, and up to 6-8 Å for carboxylates with a weak interface propensity (namely $HCOO^-$ and CH_3COO^-). Moreover, this entropic term is also at the origin of an excluded volume (corresponding to weak $P(r)$ values) observed at the center of all the droplets, even for the anions showing the weakest propensity for the droplet surface, such as $HCOO^-$. However, this volume decreases rapidly as the droplet size increases. For instance, in the case of the $HCOO^-/N_w = 1000$ droplet system, the volume of the sphere centered at the droplet COM and within which the ion location probability $P(r)$ is 10 times smaller than the maximum of $P(r)$, represents less than 3‰ of the total droplet volume.

All the ion/water PMFs have a local minimum close to the air/water interface (usually at about 2 Å from the interface, within the droplet). Such a minimum was also observed for methylated ammonium ions while it doesn't exist for monoatomic cations like K^+ [35]. We interpret it here as the first step of the solvation process of an organic ion, corresponding to the saturation of the first hydration shell of its ionic head while its alkyl groups are still weakly interacting with water (see also Figure 5). This interpretation explains why this minimum is located at the same distance from the interface for all the carboxylates considered. The PMF values for these minima, PMF_{min}, are plotted as a function of the droplet size in Figure 4. For $N_w > 50$ and for all the carboxylates, the PMF_{min} value increases with the droplet size and it rapidly converges towards its value at the air/liquid water interface, the convergence being almost achieved for $N_w = 1000$. For $N_w \leq 100$, the PMF_{min} values are all negative, showing the strong propensity of all the carboxylates for the surface of small droplets. The carboxylate ions alter thus noticeably the structure of their surrounding water, which prevents them to easily penetrate in small droplets. For the largest carboxylates, the propensity for the droplet surface remains strong up to the

air/liquid water interface (for both $C_4H_9COO^-$ and $C_5H_{11}COO^-$, their PMF_{min} values are then around -1.5 kcal mol^{-1}) while the surface propensity of the smallest carboxylates, $HCOO^-$ to $C_2H_5COO^-$, disappears as soon as $N_w = 300$. This is in line with a recent experimental study [15] showing that only carboxylate ions larger than propanoate have a marked propensity for the air/liquid water interface.

The solvation of carboxylate ions is mainly driven by rather strong electrostatic water/COO^- interactions. However, the marked difference in propensity for the interface between small and large alkylated carboxylates solvated in large water systems shows the pivotal role that a few methyl groups can play on organic ion solvation properties. As the destabilization of the water structure due to the presence of such small hydrophobic groups is overall weak (the hydration free energy of methane is +2 kcal mol^{-1}), this demonstrates that the competition between ion/water and water/water interactions can be easily altered. We may note here that the interaction energy profile for a small ion solvated in water is flat (see for instance our former results for NH_4^+ [35], as well as the below-discussed ones corresponding to $HCOO^-$). This suggests the air/water interface propensity of an organic ion to be mainly dominated by ion carbon chain/water hydrophobic effects. That explains why the trends of the carboxylate propensity for the air/liquid water interface predicted by our simulations is in line with the solvation trends of neutral hydrocarbons (see for instance the recent discussion of Ben-Amotz [43]). In other words, the present study suggests that the ionic head and the alkyl substituent of an organic ion can be considered as solvated independently.

We note a very good agreement between the PMF_{min} values corresponding to droplets with $N_w = 1000$ and to air/liquid water interfaces, for the four smallest carboxylates while these values differ by about 0.4 kcal mol^{-1} for the largest carboxylates $C_4H_9COO^-$ and $C_5H_{11}COO^-$. This difference may originate from the correction δPMF used to account for the dispersion truncation in bulk simulations, which is estimated by using a basic relation not suited for large polyatomic ions (see Section II B). However, this may also result from small differences in the large carboxylate structures in the interface vicinity between droplet and bulk systems, even if we have not been able to identify them because of the too large statistical uncertainty still affecting data extracted from 10 ns-scale simulations (see below).

C. Carboxylate orientation at the air/water interface

To investigate the effects of solvation on the orientation and on the structure of alkylated carboxylates, especially in the vicinity of the air/water interfaces, we consider two main kinds of geometric parameters, namely the distances R_C between the carbon atom of the carboxylate CH_3 group and the droplet COM (or simulation cell SCC) in large water systems, and the carboxylate dihedral angles Ψ_n. Below, the intramolecular axis between the carbon atoms of the COO^- and of the CH_3 moieties is denoted by $\mathbf{L}_{CC}$. Its norm in gas phase is denoted by L_{CC}, and its values are 1.5, 3.3, 3.9 and 4.9 Å from ethanoate to hexanoate, respectively (see Section III A 1).

For the $N_w = 1000$ droplet systems (radii around 20 Å), the averaged quantities $\Delta\bar{R}_C = \bar{R}_C - d_c$ and the root mean square deviations $\delta\bar{R}_C$ of R_C are plotted vs. the distances d_c in Figure 6. These profiles are very close to the profiles computed at the air/liquid water interface (see Supporting Information). Regardless of the carboxylate ion, we identify two main regimes for $\Delta\bar{R}_C$. In the vicinity of the droplet core, the orientation of $\mathbf{L}_{CC}$ is random ($\Delta\bar{R}_C \approx L_{CC}$ at the droplet core, i.e., when $d_c = 0$) and then, it decreases down to zero as d_c increases. However, starting at about 10 Å before the air/water interface, the axis $\mathbf{L}_{CC}$ is more and more oriented orthogonally to the interface, i.e., $\Delta\bar{R}_C$ converges towards a maximum value (around $+L_{CC}$) reached about 4-5 Å before the interface. Close to the air/water interface, the carboxylate orientation is thus strongly constrained. The COO^- moiety points towards the aqueous core while the alkyl chain is repelled from it. As shown by the $\delta\bar{R}_C$ plots, this structural constraint is particularly strong in a shell of 3 Å before the droplet boundary for all the alkylcarboxylates (in this domain, $\delta\bar{R}_C \leq 2$ Å).

Some examples of distributions of the dihedral angles Ψ_n, g_{Ψ_n}, computed along simulations at the air/liquid water interface are provided as Supporting Information for the hexanoate. For all of the carboxylates, the g_{Ψ_n} functions present three sharp peaks at 120, 180 and 240°, allowing one to compute the ratios p_{Ψ_n} between anti and gauche conformations, for each dihedral angle Ψ_n. These ratios computed from air/liquid water simulation data are plotted vs. d_c for the three largest carboxylates in Figure 7. Profiles very close to the latter ones are computed from $N_w = 1000$ droplet data (see Supporting Information). First, by comparing the p_{Ψ_n} values within the bulk and in the gas phase (but far from the air/water interface), they seem to be still affected by relatively large uncertainties, as

shown by the marked discontinuous profiles of p_{Ψ_n}. These statistical uncertainties prevent us to discuss the possible weak structural changes affecting large carboxylates when crossing air/water interfaces. Nevertheless, the hexanoate p_{Ψ_n} profiles show that the carboxylate dihedral angles Ψ_5 and Ψ_6 (corresponding exclusively to methyl carbon atoms) are slightly altered when crossing the air/water interface while the dihedral angle Ψ_4 (whose first carbon atom belongs to the COO^- moiety) is more sensitive to the solvent effects. For instance, the ratio p_{Ψ_4} increases from about 1:6 in gas phase to 1:4 in the bulk, with a maximum of 1:3 in the vicinity of the air/water interface for hexanoate, showing that the anti conformation for Ψ_4 is favored by the solvent effects. For such a large anion, that may be interpreted as allowing more water molecules to interact with the carboxylate anionic head in solution. However, the dependence of dihedral angles Ψ_4 on the chemical environment seems to be less accented for the smallest carboxylate ions (see for instance the profiles plotted in Figure 7 for pentanoate).

D. Microscopic interactions occurring in ion solvation

Along each umbrella sampling simulation, we computed the ion/water mean energy $\bar{U}^{iw}(d_c)$ and its components $\bar{U}^{iw}_{rep}(d_c)$, $\bar{U}^{iw}_{qq'}(d_c)$, $\bar{U}^{iw}_{pol}(d_c)$, $\bar{U}^{iw}_{shb}(d_c)$ and $\bar{U}^{iw}_{disp}(d_c)$, as well as the water/water interaction mean energy $\bar{U}^{ww}(d_c)$. The results for ions in $N_w = 600$ water droplets, as a function of ion/COM distance d_c, are illustrated in Figure 8 for six carboxylate ions. As in the case of ammonium ions and for all the droplet systems, the root mean square deviation of $\bar{U}^{iw}(d_c)$ is about 6 kcal mol^{-1} and the uncertainty affecting the $\bar{U}^{ww}(d_c)$ values and tied to droplet evaporation effects is at most 5 kcal mol^{-1}. Below, we denote by $\bar{U}^{yy}_{xx}$ the average of the energy component $\bar{U}^{yy}_{xx}(d_c)$ scaled by the probability density $P(d_c)$ of finding an ion at a position d_c during a simulation.

The $\bar{U}^{iw}_{qq'}(d_c)$ and $\bar{U}^{iw}_{shb}(d_c)$ profiles in Figure 8 are very similar for all the alkylated carboxylates. This result was expected for $\bar{U}^{iw}_{shb}(d_c)$, as it corresponds to a short-range energy term centered on the COO^- oxygen atoms. For the Coulombic components $\bar{U}^{iw}_{qq'}(d_c)$, that arises from the strong electrostatic charges located on the COO^- moiety, which mainly drive the Coulombic ion/water interactions (we assume that the charges on the COO^- oxygens are equal for all of the carboxylate ions).

Ion/water dispersion becomes stronger when the carboxylate side chain is longer. Each

added methylene group adds an ion/water dispersion energy $\bar{U}^{iw}_{disp}(d_c)$ of -3 kcal mol^{-1}. Similarly, the ion/water repulsion and the water/water energies $U^{iw}_{rep}(d_c)$ and $U_{ww}(d_c)$ also change regularly with each new methylene group but oppositely, with a destabilizing effect, each adding a positive interaction energy of 1 kcal mol^{-1} per group. Lastly, the ion/water polarization destabilizes (increases the energy) the ion/water interactions within a droplet. The strength of this destabilization also increases with the alkyl chain length, adding +0.6 kcal mol^{-1} per CH_2 group, but not linearly as for ion/water repulsion. In particular, $U^{iw}_{pol}(d_c)$ seems to already converge for pentanoate.

For $\bar{U}^{iw}_{disp}(d_c)$, the stabilization of -3 kcal mol^{-1} per added CH_2 group may result from two weak CH$\cdots$ solvent hydrogen bond interactions (thus of -1.5 kcal mol^{-1}). This effect is comparable, within the usual 1 kcal/mol uncertainty of these estimates, to the cluster-based analysis for alkyloxonium and alkylammonium ions, where each CH$\cdots$ solvent interaction adds about -2.5 kcal mol^{-1} to the hydrophobic solvation enthalpy (i.e., each CH_2 group adds -5 kcal mol^{-1})[44, 45]. This similarity suggests that $\bar{U}^{iw}_{disp}(d_c)$ is a significant factor in hydrophobic solvation. Interestingly, the similar effect for the onium cations and carboxylate anions suggests then that the hydrophobic solvation energy per CH hydrogen may also apply to the solvation of alkyl groups of alkylated neutral molecules.

As already reported in earlier studies [35, 46, 47], water molecules jump from the droplet onto the ions at the water surface. That explains why the short-range ion/water energies like $\bar{U}^{iw}_{rep}(d_c)$ and $\bar{U}^{iw}_{shb}(d_c)$ don't converge towards zero ouside of the droplet. Concerning $HCOO^-$, most of its ion/water energy components behave as in the case of the alkylated carboxylates. The differences between the $HCOO^-$ and alkylated data may be interpreted as resulting from the $HCOO^-$ small size allowing more water molecules to interact with it at short range.

Interestingly, the sum of the total ion/water and the water/water interaction energies $\bar{U}^{iw}(d_c)$ and $\bar{U}^{ww}(d_c)$ at the droplet core is very close regardless of the alkylated carboxylate size, within less than 2 kcal mol^{-1} in the particular case of $N_w = 600$ droplet systems for $d_c < 8$ Å (see Fig. 8). However, this sum is weaker and weaker as the anion size increases, showing that enthalpic effects seem to favor the hydration of large carboxylates. Hence, their larger propensity for the air/water interface, relative to the small carboxylates, has an entropic origin (like the perturbation of water molecule HB networks at the vicinity of the anion carbon chains [48]).

As for ammonium ions and K^+, and for all the carboxylates, Coulombic and dispersion ion/water interactions are centripetal (as well as the specific carboxylate/water U^{iw}_{shb} term), whereas ion/water polarization and repulsive effects are centrifugal. Moreover, the water structure reorganization induced by the carboxylate ion presence leads also to centrifugal forces, as in the ammonium and K^+ case. That shows the ion solvation process to be controlled by the same microscopic forces, regardless of the nature of the ion. In particular, ion/water polarization effects systematically disadvantage ion solvation inside the droplets and favors the ionic interface propensity. That clearly shows the necessity to accurately model ion/water polarization for a proper description of ions at air/water interfaces, in agreement with earlier findings [28–30]. Nevertheless, the weights of the different ion/water interaction terms can largely differ according to the ion nature. For instance, if all the water/water interaction energies $\bar{U}^{ww}$ are less stable in ion/droplet systems than in pure water droplets, the water destabilization energies (i.e., the differences in the $\bar{U}^{ww}$ energies between ion/droplet and pure water droplet systems) are larger for carboxylates than for ammonium ions, by 50% (about 15 kcal mol^{-1}).

E. Effects of hydrocarbon chain lengths on solvation enthalpies and entropies

The incremental effects of added CH_2 groups on ion solvation enthalpies can be evaluated quantitatively by comparing for example the shortest and longest alkylated carboxylates in Figure 8 (*i.e.* ethanoate and hexanoate interacting with a 600 water droplet). Note that even if the uncertainty affecting the water/water interaction enthalpies is about 5 kcal mol^{-1} because of evaporation effects (see above), the smoothed water/water interaction enthalpies shown in Figure 8 can be considered reliable within about $\pm$ 1 kcal mol^{-1}. Moreover, the values discussed below agree with those computed from 1000 water droplet data within less than 1 kcal mol^{-1}.

Figure 8**A** shows that the total ion/water interaction enthalpy U_{iw} near the droplet COM for hexanoate is more negative by 5 kcal mol^{-1} than for ethanoate, i.e., ΔU_{iw}(hex-eth) = -5 kcal mol^{-1}. However, the water/water interaction enthalpy difference varies oppositely, as ΔU_{ww}(hex - eth) = + 3 kcal mol^{-1}. Hence the difference between the solvation enthalpies of hexanoate and ethanoate inside the droplet is then $\Delta U^{\rm COM}_{solv}$(hex - eth) = ΔU_{iw}(hex-eth) +ΔU_{ww}(hex - eth) = -2 kcal mol^{-1}. In comparison, the Figure 8 data at the droplet

surface lead to ΔU_{iw}(hex - eth) = +2 kcal mol^{-1} and to $\Delta U_{ww}^{\text{surface}}$(hex - eth) = 0. The total difference between the solvation enthalpies of hexanoate and ethanoate at the surface is thus $\Delta U_{solv}^{\text{surface}}$(hex - eth) = +2 kcal mol^{-1}.

Hence, the total calculated solvation enthalpy is more negative (stabilizing) for hexanoate than for ethanoate by 2 kcal mol^{-1} inside the droplet, where the ionic groups and hydrocarbon chains are fully solvated, while the solvation enthalpy is less stabilizing (more positive) for hexanoate than for ethanoate at the droplet surface by 2 kcal mol^{-1}. Hence, moving the anions from the droplet core to the droplet surface is more endothermic by 4 kcal mol^{-1} for hexanoate than for ethanoate. From the data summarized in Supporting Information, the latter difference is mainly due to methylene/water dispersion effects, in agreement with earlier studies showing that the electrostatic organic ion/water term does not vary significantly with alkyl size, but the solvation enthalpies of the neutrals does vary with alkyl size [49, 50].

By these enthalpy effects hexanoate should have a higher affinity for the interior than ethanoate. However, our simulations show that hexanoate has a higher propensity for the air/liquid water interface than ethanoate. That suggests thus an additional positive entropy effect in moving hexanoate from the droplet core to the droplet surface, to make the free energy of transfer to the surface negative (because of the PMF definition, see Equation equ:prob-droplet, this entropic effect is different from the TS_{geom} one discussed above). This new effect can be associated with the loss of structure-making effect of hydrocarbon solutes on surrounding water (here, structure-making $\text{CH}\cdots\text{OH}_2$ hydrogen bonds in ion solvation lead to a compensating enthalpy/entropy effect common in thermochemistry). Quantitatively, the above results suggests that adding 4 CH_2 groups from ethanoate to hexanoate needs to contribute, for moving the ion to the surface, a desolvation entropic term $\text{T}\Delta\text{S}_{alkyl}$ of $>$ 4 kcal mol^{-1}, or $>$ 1 kcal mol^{-1} per CH_2 group (that corresponds to a solvation entropy change of $<$ -3.3 cal mol^{-1} K^{-1} per CH_2 group). The latter value is in line with the solvation entropy values reported experimentally for $n-$propanoate and $n-$butanoate, which are more negative than ethanoate by -4.3 and -7.7 cal mol^{-1} K^{-1} [50], respectively.

F. Ion/water droplet solvation energy: convergence towards bulk limit

The mean ion/water droplet energies $\bar{U}^{iw}$ are plotted as a function of the droplet size N_w in Figure 9 for all the carboxylate ions. While they are all very similar for the smallest droplet $N_w = 50$, their behavior differ then for the different carboxylates in larger droplets. Nevertheless, we note that all of the values $\bar{U}^{iw}$ for alkylated carboxylates seem to converge towards the same value $\bar{U}^{iw}(\infty)$ for $N_w \to \infty$. This convergence is a priori faster for the smallest alkylated carboxylates. To extrapolate the value $\bar{U}^{iw}(\infty)$ from quasi-spherical droplet data for a small polyatomic ion, a standard approach consists in fitting the $\bar{U}^{iw}(N_w)$ data to the power-law function of N_w

$$\bar{U}^{iw}(N_w) = \bar{U}^{iw}(\infty) + \epsilon_0/(N_w + a)^{1/3} + \epsilon_1/(N_w + a)^{2/3}. \quad (15)$$

Here, $\bar{U}^{iw}(\infty)$, ϵ_0, ϵ_1 and a are adjustable parameters. As all the water droplets are quasi-spherical, the quantity $(N_w + a)^{1/3}$ is a measure of the droplet radius R_d, and a is the ratio between the ion effective volume and the solvent one. Lastly, the fourth term of Equation 15 is introduced to account for a non-symmetric charge distribution in an ion, like for the carboxylates (see Figure 1). As discussed in Ref. 51 and for the droplet size considered here, the above-mentioned equation can be used regardless of the ion propensity for the droplet interior (or surface). However, because of the size of our droplet systems (their radii are at most around 20 Å), this equation is expected to provide reliable results only for the smallest carboxylates.

In our former study dealing with methylated ammonium cations and K^+, we extrapolated the $\bar{U}^{iw}(\infty)$ values by setting the parameters a and ϵ_1 to zero. To assess the reliability of these former results and the ability of such a fitting function to extrapolate bulk values, we fitted our former cation data and the carboxylate ones by considering three different kinds of functions, for which the parameters a and ϵ_1 are set to zero individually or together. All of the new extrapolated $\bar{U}^{iw}(\infty)$ values are summarized in Table II.

For all the cations, the results summarized in Table II clearly show that the choice of the fitting function has no effect on the extrapolated $\bar{U}^{iw}(\infty)$ values, which differ in this case by 1.2 kcal mol^{-1} on average. For the smallest carboxylates $HCOO^-$ and CH_3COO^-, the $\bar{U}^{iw}(\infty)$ values are also almost insensitive to the fitting functions, as they differ by less than 2 kcal mol^{-1} on average. For these carboxylate ions, we may even note a much better agreement among the $\bar{U}^{iw}(\infty)$ values computed by not setting both a and ϵ_1 to zero. In this

case, their $\bar{U}^{iw}(\infty)$ values differ only by about 1 kcal mol $^{-1}$ on average. For the largest carboxylates ($>$ CH_3COO^-), the $\bar{U}^{iw}(\infty)$ values are clearly more sensitive to the choice of the fitting function. For them, the extrapolated values differ by about 5 kcal mol^{-1} on average. Hence, our extrapolation protocol to estimate the ion/water interaction energies in liquid water appears to be robust enough only for small ions, regardless of their nature while for large ions, in particular with a long linear alkyl chain, this protocol provides only a crude estimate of the latter interaction energy, at least when considering the present droplet sizes. Nevertheless, we note that the $\bar{U}^{iw}(\infty)$ values for all the alkylcarboxylates are more stable than the $CH_3NH_3^+$ one by about 20% (25 kcal mol^{-1}), regardless of the fitting function used.

The water destabilization energy values, $\Delta\bar{U}^{ww}_{\rm bulk}$, are constant within 1 kcal mol^{-1} for both the cations and the anions. However, these energies are stronger by 35% for the carboxylates than for the ammonium ions and K^+ (that represents a difference in $\Delta\bar{U}^{ww}_{\rm bulk}$ around 13 kcal mol^{-1}). Hence, carboxylates affect more strongly the water structure in their vicinity than ammonium and K^+ ions. This stronger solvent destabilization induced by carboxylates leads to cancel out most of the differences in the ion/water interaction energies $\bar{U}^{iw}(\infty)$ between carboxylates and the latter cations. Hence, as experimentally reported [50, 52, 53], our simulation results show that the single ion absolute solvation enthalpies $\Delta H_{g\to aq}$, computed according to

$$\Delta H_{g\to aq} = \bar{U}^{iw}(\infty) + \Delta\bar{U}^{ww}_{\rm bulk} + \Delta\bar{U}^{\rm ion}_{\rm intra} - k_B{\rm T}, \qquad (16)$$

are all very close within a few kcal mol^{-1} for the smallest ions $HCOO^-$, CH_3COO^-, NH_4^+, $CH_3NH_3^+$, and K^+. These computed enthalpies are slightly overestimated on average, relative to experiment, by about 2.5 kcal mol^{-1} (see Table II). However for CH_3COO^-, our $\Delta H_{g\to aq}$ value is in better agreement with experiment (about -90 kcal mol^{-1} [19, 20, 52]) than the values reported in previous theoretical studies that predicted: -80 kcal mol^{-1} [19, 24] and -87 kcal mol^{-1} [20] by using pairwise forcefields, and -87 kcal mol^{-1} [24] with a polarizable forcefield. Nevertheless, for larger carboxylates, our $\Delta H_{g\to aq}$ estimates differ more noticeably compared to experimental values, from about 5 to 10 kcal mol^{-1}. As already discussed above, the extrapolation schemes we used appear to be not robust enough for large carboxylates, which prevents us to further discuss the discrepancies between simulated and experimental $\Delta H_{g\to aq}$ values.

To assess the accuracy of our computational protocol to model the carboxylate hydration, we may also consider the proton absolute solvation enthalpy $\Delta H_{g\to aq}(H^+)$, derived

from the experimental data summarized in Table I, the experimental carboxylate single-ion solvation energies from Ref. [52] or the present computed values, according to the following thermochemical cycle

$$\Delta H_{g\to aq}(\mathrm{H^+}) = \Delta H_{g\to aq}(\mathrm{BH}) + \Delta H^0_{aq,\mathrm{dissociation}}(\mathrm{BH}) - \Delta H_{g\to aq}(\mathrm{B^-}) + \Delta H^{prot}_g(\mathrm{B^-}) \quad (17)$$

Because of the lack of thermochemical data for hexanoate, we consider for it the same experimental data as for pentanoate. When using our simulation results, the carboxylate-based values $\Delta H_{g\to aq}(\mathrm{H^+})$ range mainly between 257 and 270 kcal mol^{-1}. These values are clearly underestimated compared to the well-accepted experimental range of values, 271-275 kcal mol^{-1} [44, 45, 54], and to the value corresponding to the experimental carboxylate single solvation energies summarized in Table II, 271.5 $\pm$ 0.2 kcal mol $^{-1}$.

However, by considering only the data of the smallest carboxylates $\mathrm{HCOO^-}$ and $\mathrm{CH_3COO^-}$, *i.e.* the ones for which the extrapolated values $\bar{U}^{iw}(\infty)$ appear to be the most reliable, we note then a better agreement between the theoretical and the experimental $\Delta H_{g\to aq}(\mathrm{H^+})$ estimates. In particular, by considering the data computed from non-zero parameters a and ϵ_1, the mean $\Delta H_{g\to aq}(\mathrm{H^+})$ value is around 269 kcal mol^{-1} for these small carboxylates. That value corresponds to the lower limit of the experimental estimates and it agrees with the value computed from methylated ammonium data, around 272 kcal mol^{-1}. As already mentioned, we computed the water destabilization energies $\Delta\bar{U}^{ww}_{\mathrm{bulk}}$ in our previous study [35] dealing with ammonium ions from simulations performed using classical Ewald summation techniques for neat water and the Particle Mesh Ewald method for ionic solutions. The values reported in Table II are computed by comparing results computed using the same Ewald protocol, which explains the small difference between the value reported here for the cation-based $\Delta H_{g\to aq}(\mathrm{H^+})$ and the previous one (270.6 kcal mol^{-1}).

The short-range stabilizing carboxylate/water interactions are modeled by considering two energy terms, namely U^{disp} and U^{shb}, for which it is not obvious to evaluate the correct ratio, as well as the strength of the anti-cooperative character of U^{shb}. In particular, the amount of destabilizing energy due to the anti-cooperative component of U^{shb} is about 7 kcal mol^{-1} for the $\mathrm{HCOO^-}/N_w = 1000$ droplet system. Hence, a slightly more anti-cooperative U^{shb} carboxylate/water energy term may destabilize the carboxylate $\Delta H_{g\to aq}$ by a few more kcal mol^{-1}, leading then to a better agreement between experiment and small carboxylate simulation-based data for the proton solvation enthalpy. However, because of the uncertainty

tied to the protocol we used to extrapolate bulk ion/water interaction energies from droplet simulations, especially for large carboxylates, data corresponding to droplet systems much larger than the ones considered here might also help to further discuss this particular point.

IV. CONCLUSIONS

We presented simulations concerning six linear alkylated carboxylates (from methanoate to hexanoate) solvated in water droplets comprising from $N_w = 50$ to 1000 water molecules and in bulk water, as well as interacting at the air/liquid water interface. The simulation protocol is based on a polarizable model including, in particular, a specific short-range many-body anisotropic energy term to accurately model the ion/water interactions. The results show that all the carboxylates have a strong propensity for the air/water interface in the case of small droplet systems ($N_w < 300$) while only carboxylates larger than propanoate have a noticeable propensity for the air/water interface in larger water droplets and at the air/liquid water interface. This is in line with recent experimental results [15]. However, as our simulations neglect acid/base phenomena, to further compare our results concerning the behavior of carboxylates at the air/water interface to experiment, a similar theoretical study of the solvation of neutral carboxylic acid needs to be performed.

Concerning carboxylate/water interactions, our calculations for 600 water droplets for example show that transferring an ion from the solution to the air/water interface is more endothermic for hexanoate than for ethanoate by 4 kcal mol^{-1}. Nevertheless, ethanoate remains in the solution while hexanoate is on the surface. This implies a positive entropy change for moving the ion to the surface, by at least 3.3 cal mol^{-1} K^{-1} per CH_2 group. Both the enthalpy and entropy effects are consistent with the loss of the structure-making effects of the alkyl chain by removal from solution. The largest factor in this effect is the difference in hydrocarbon/water dispersion energy, which is more negative for hexanoate than ethanoate by 12 kcal mol^{-1}, *i.e.* each CH_2 group contributes 3 kcal mol^{-1} to the ion-water dispersion enthalpy. Further, comparable effects of alkyl groups were observed in the solvation of methylated ammonium ions, suggesting that the ionic head-groups and alkyl substituents are solvated as independent solutes.

As already reported for methylated ammonium ions and for K^+ [35], the present results show also that the ion/water polarization forces are centrifugal while the ion/water disper-

sion and Coulombic forces are centripetal in carboxylate/water droplets. Together, all of these results show the propensity of an ion for aqueous interfaces (regardless of wether it is a monoatomic cation or an alkylated cation or anion) to result from a complex interplay of microscopic forces, like the above-mentioned three ones. That also demonstrates the necessity for explicitly and accurately accounting for ion/water polarization effects to perform reliable simulations of an ion interacting close to an aqueous interface, as already discussed by several authors [28–30].

The obtained carboxylate/droplet data allow us also to extrapolate the single carboxylate absolute solvation enthalpies and thus to estimate the proton absolute solvation enthalpy. By considering the data concerning the smallest carboxylates (methanoate and ethanoate), the present carboxylate-based proton solvation enthalpy is about 269 kcal mol^{-1}, a value in good agreement with the experimental one (ranging from 271 to 275 kcal mol^{-1}) and the value that we reported using the same computational protocol for methylated ammonium ions [35] (about 271 kcal mol^{-1}). For the largest carboxylate ions, the droplet data yield a proton solvation enthalpy largely underestimated, up to 10 kcal mol^{-1}, relative to experiment. To our opinion, that results mainly from the data set we used, which corresponds to droplet systems still too small (in particular, when we compare the droplet size to the size of the largest carboxylates like pentanoate and hexanoate). That can prevent us to extrapolate reliable results by using simple power-law functions of the droplet size as done here. This point needs thus to be further discussed, in particular by considering new results concerning larger ion/droplet systems (including around 10 000 water molecules and more). Such simulations are still computationally demanding even by using forcefield-based approaches. Nevertheless, they will provide important informations allowing one to better quantify the impact of enthalpic effects (like the electrostatic interactions between water and an ionic head) and of entropic ones (which mainly drive the hydration of small hydrophobic solutes [48]) on the hydration properties of organic ions.

SUPPORTING INFORMATION AVAILABLE

Full description of the quantum computations, of the model parameter assignment strategy, of the molecular dynamics details and of data mentioned in the text. This material is available free of charge via the Internet at http://pubs.acs.org.

ACKNOWLEDGMENTS

We thank Othman Bouizi and Emmanuel Oseret (Exascale Computing Research Laboratory, a joint INTEL/CEA/UVSQ/GENCI laboratory) for their help in optimizing the code POLARIS(MD). We acknowledge an access to the supercomputing systems of the CCRT (Centre de Calcul et de Recherche Technologique) of the French Nuclear Agency (CEA), and the use of the Stampede supercomputing system at TACC/UT Austin, funded by NSF award OCI-1134872.

---

[1]

[2] Finlayson-Pitts, B. J. *Chemical Reviews* **2003,** *103,* 4801-4822.

[3] Finlayson-Pitts, B. J. *Phys. Chem. Chem. Phys.* **2009,** *11,* 7760-7779.

[4] Warshel, A.; Sharma, P. K.; Kato, M.; Xiang, Y.; Liu, H.; Olsson, M. H. M. *Chemical Reviews* **2006,** *106,* 3210-3235.

[5] Jungwirth, P.; Winter, B. *Annual Review of Physical Chemistry* **2008,** *59,* 343-366.

[6] McGorty, R.; Fung, J.; Kaz, D.; Manoharan, V. N. *Materials Today* **2010,** *13,* 34 - 42.

[7] Mishra, H.; Enami, S.; Nielsen, R. J.; Stewart, L. A.; Hoffmann, M. R.; Goddard, W. A.; Colussi, A. J. *Proceedings of the National Academy of Sciences* **2012,** *109,* 18679-18683.

[8] Prisle, N. L.; Raatikainen, T.; Laaksonen, A.; M., B. *Atmos. Chem. Phys.* **2010,** *10,* 5663-5683.

[9] Gojlo, E.; Śmiechowski, M.; Panuszko, A.; Stangret, J. *The Journal of Physical Chemistry B* **2009,** *113,* 8128-8136.

[10] Kameda, Y.; Ebata, H.; Usuki, T.; Uemura, O.; Misawa, M. *Bull. Soc. Chem. Jpn.* **1994,** *67,* 3159–3164.

[11] Kameda, Y.; Mori, T.; Nishiyama, T.; Usuki, T.; Uemura, O. *Bull. Soc. Chem. Jpn.* **1996,** *69,* 1495–1504.

[12] Kameda, Y.; Fukahara, K.; Mochiduki, K.; Naganuma, H.; Usuki, T.; Uemura, O. *J. Non-Cryst. Solids* **2002,** *312-314,* 433–437.

[13] Rahman, H. M. A.; Hefter, G.; Buchner, R. *The Journal of Physical Chemistry B* **2012,** *116,* 314-323.

[14] Rahman, H. M. A.; Hefter, G.; Buchner, R. *The Journal of Physical Chemistry B* **2013,** *117,* 2142-2152.

[15] Ottosson, N.; Wernersson, E.; Soderstrom, J.; Pokapanich, W.; Kaufmann, S.; Svensson, S.; Persson, I.; Ohrwall, G.; Bjorneholm, O. *Phys. Chem. Chem. Phys.* **2011,** *13,* 12261-12267.

[16] Leung, K.; Rempe, S. B. *Journal of the American Chemical Society* **2004,** *126,* 344-351.

[17] Payaka, A.; Tongraar, A.; Rode, B. M. *The Journal of Physical Chemistry A* **2009,** *113,* 3291-3298.

[18] Payaka, A.; Tongraar, A.; Rode, B. M. *The Journal of Physical Chemistry A* **2010,** *114,* 10443-10453.

[19] Alagona, G.; Ghio, C.; Kollman, P. *Journal of the American Chemical Society* **1986,** *108,* 185-191.

[20] Jorgensen, W. L.; Gao, J. *Journal of Physical Chemistry* **1986,** *90,* 2174-2182.

[21] Minofar, B.; Vácha, R.; Wahab, A.; Mahiuddin, S.; Kunz, W.; Jungwirth, P. *The Journal of Physical Chemistry B* **2006,** *110,* 15939-15944.

[22] Minofar, B.; Jungwirth, P.; Das, M. R.; Kunz, W.; Mahiuddin, S. *The Journal of Physical Chemistry C* **2007,** *111,* 8242-8247.

[23] Mahiuddin, S.; Minofar, B.; Borah, J. M.; Das, M. R.; Jungwirth, P. *Chemical Physics Letters* **2008,** *462,* 217 - 221.

[24] Meng, E. C.; Kollman, P. A. *The Journal of Physical Chemistry* **1996,** *100,* 11460-11470.

[25] Liang, T.; Walsh, T. R. *Phys. Chem. Chem. Phys.* **2006,** *8,* 4410-4419.

[26] Chang, T.-M.; Dang, L. X. *Chemical Reviews.* **2006,** *106,* 1305–1322.

[27] Jungwirth, P.; Tobias, D. J. *Chemical Reviews* **2006,** *106,* 1259-1281.

[28] Wick, C. D. *J. Chem. Phys.* **2009,** *131,* 084715.

[29] Wick, C. D.; Cummings, O. T. *Chem. Phys. Lett.* **2011,** *513,* 161-186.

[30] Netz, R. R.; Horinek, D. *Annu. Rev. Phys. Chem.* **2012,** *63,* 401-418.

[31] Simon, A.; Iftner, C.; Mascetti, J.; Spiegelman, F. *The Journal of Physical Chemistry A* **2015,** *119,* 2449-2467.

[32] Consta, S.; Oh, M. I.; Soltani, S. *International Journal of Mass Spectrometry* **2015,** *377,* 557 - 567 Special Issue: {MS} 1960 to Now.

[33] Réal, F.; Vallet, V.; Flament, J.-P.; Masella, M. *J. Chem. Phys.* **2013,** *139,* 114502.

[34] Trumm, M.; Guerrero Martinez, Y. O.; Réal, F.; Schimmelpfennig, B.; Masella, M.; Vallet, V. *J. Chem. Phys.* **2012,** *136,* 044509.

[35] Houriez, C.; Meot-Ner (Mautner), M.; Masella, M. *The Journal of Physical Chemistry B* **2014,** *118,* 6222-6233.

[36] Saykally, R. *Nature Chemistry.* **2013,** *5,* 82-84.

[37] "Gaussian 09 Revision D.01", Gaussian Inc. Wallingford CT 2009.

[38] Réal, F. personal communication.

[39] Thole, B. *Chem. Phys.* **1981,** *59,* 341-350.

[40] Brooks, B. *et al. J. Comput. Chem.* **2009,** *30,* 1545-1615.

[41] Allen, F. H. *Acta Crystallographica Section B* **2002,** *58,* 380–388.

[42] Kondo, T.; Miyazaki, Y.; Inaba, A.; Koga, Y. *The Journal of Physical Chemistry B* **2012,** *116,* 3571-3577.

[43] Ben-Amotz, D. *The Journal of Physical Chemistry Letters* **2015,** *6,* 1696-1701.

[44] Meot-Ner, M. *J. Phys. Chem.* **1987,** *91,* 417-426.

[45] Meot-Ner (Mautner), M. *Chem. Rev.* **2005,** *105,* 213-284.

[46] Caleman, C.; Hub, J.; van Maaren, P.; van der Spoel, D. *Proc. Natl. Acad. Sci. USA.* **2011,** *108,* 6838-6842.

[47] Dang, L. X.; Chang, T.-M. *J. Phys. Chem. B* **2002,** *106,* 235-238.

[48] Chandler, D. *Nature* **2005,** *437,* 640–647.

[49] Aue, D. H.; Webb, H. M.; Bowers, M. T. *Journal of the American Chemical Society* **1976,** *98,* 318-329.

[50] Meot-Ner, M.; Sieck, L. W. *Journal of the American Chemical Society* **1986,** *108,* 7525-7529.

[51] Peslherbe, G. H.; Ladanyi, B. M.; Hynes, J. T. *J. Phys. Chem. A* **1999,** *103,* 2561-2571.

[52] Wilson, B.; Georgiadis, R.; Bartmess, J. E. *Journal of the American Chemical Society* **1991,** *113,* 1762-1766.

[53] Meot-Ner (Mautner), M. *Chem. Rev.* **2012,** *112,* PR22-PR103.

[54] Tuttle, T. R.; Malaxos, S.; Coe, J. V. *J. Phys. Chem. A* **2002,** *106,* 925-932.

FIGURES

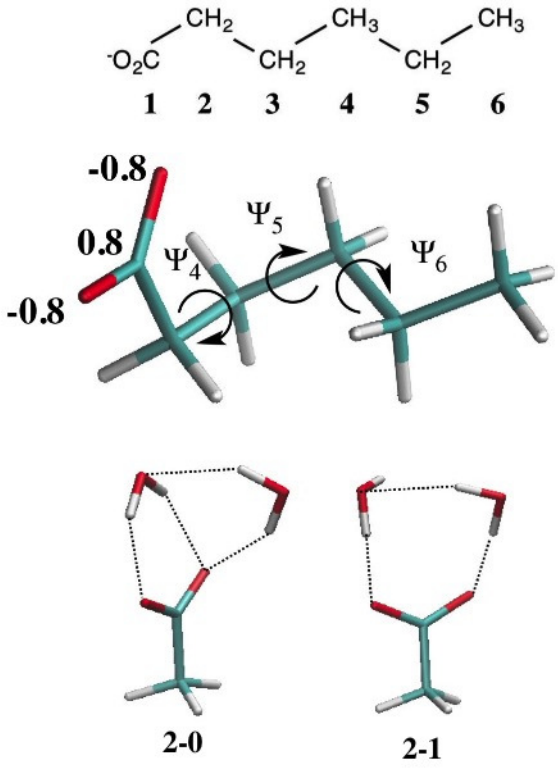

807

808 FIG. 1. Top: Labeling of carbon atoms in the carboxylates (bold characters). Middle: the most
809 stable structure of hexanoate (according to our model, the three dihedral angles Ψ_n are of 66.6,
810 49.6 and 177.8°, for n = 4-6, respectively). The numbers shown close to the hexanoate anionic
811 head are the model electrostatic charges, in e. Bottom: the two $CH_3COO^-/(H_2O)_2$ structures **2-0**
812 and **2-1**.

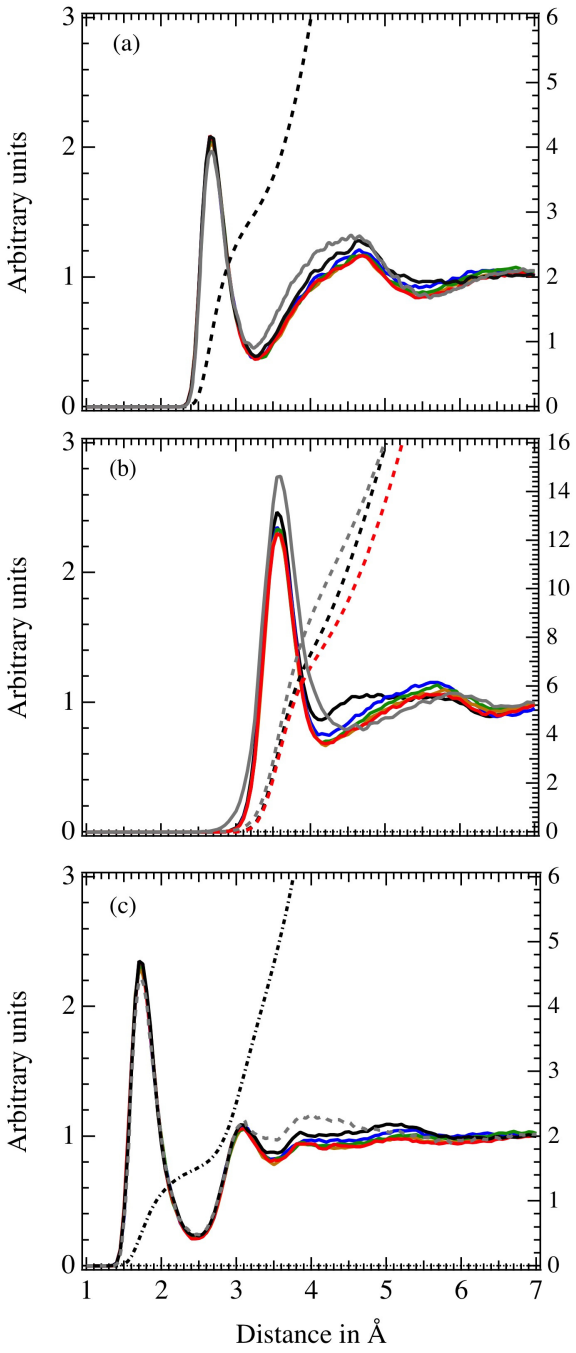

FIG. 2. Carboxylate/water radial distribution functions: $g_{\mathrm{OO_w}}$ (a), $g_{\mathrm{CO_w}}$ (b), and $g_{\mathrm{OH_w}}$ (c). Grey line: methanoate; black: ethanoate; blue: propanoate; green: butanoate; orange: pentanoate; red: hexanoate. Corresponding dashed lines: some examples of integrated radial distribution functions. $g_{\mathrm{OO_w}}$ and $g_{\mathrm{OH_w}}$ are averaged over the carboxylate oxygen atoms and the water hydrogen atoms.

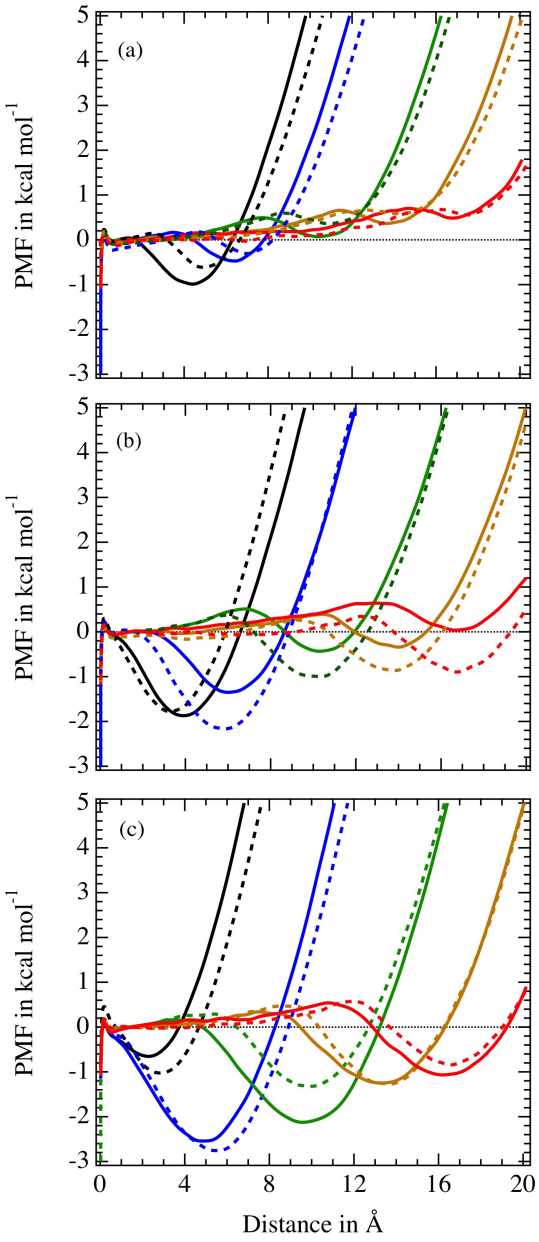

FIG. 3. Carboxylate/water droplet PMF. (a): $HCOO^-$ (—) and CH_3COO^- (- -); (b): $C_2H_5COO^-$ (—) and $C_3H_7COO^-$ (- -); (c): $C_4H_9COO^-$ (—) and $C_5H_{11}COO^-$ (- -). Black: $N_w = 50$; blue: $N_w = 100$; green: $N_w = 300$; orange: $N_w = 600$; red: $N_w = 1000$.

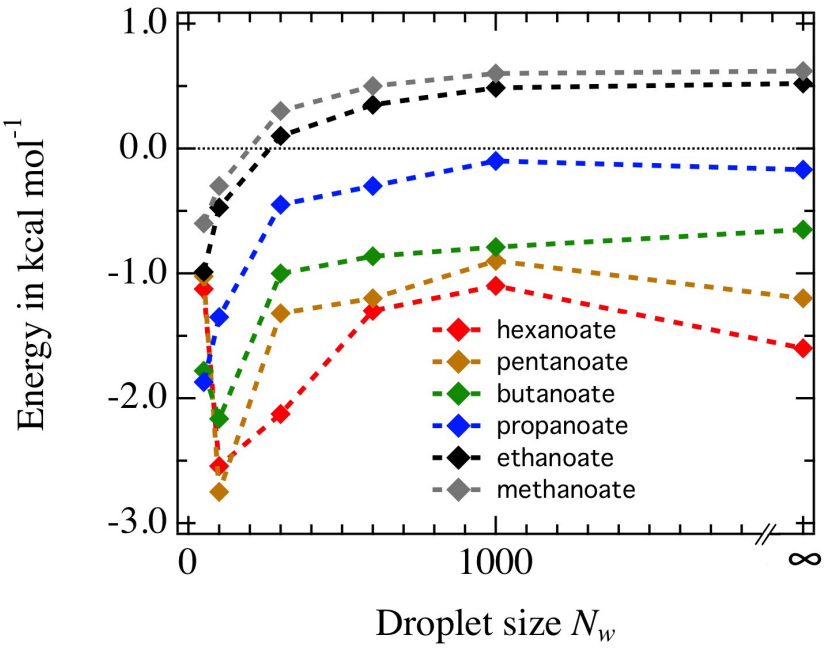

822

823 FIG. 4. PMF values at the minimum close to the air/droplet interfaces as a function of the droplet
824 size. The bulk values (∞) are computed from air/liquid water simulations and by accounting for
825 the corrections δPMF (see Equation 11).

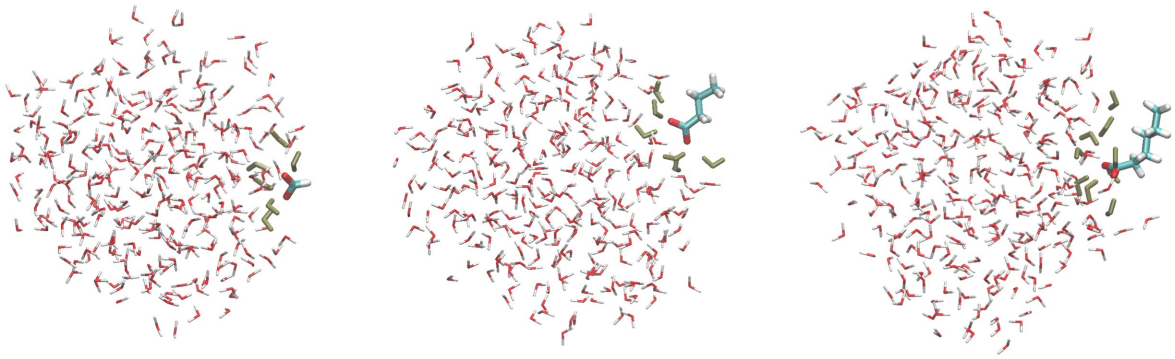

826

827 FIG. 5. Some simulation snapshots showing representative structures corresponding to the PMF
828 minimum values close to the droplet boundary. Methanoate, butanoate and hexanoate, respec-
829 tively, interacting with a $N_w = 300$ droplet. The water molecules of the first hydration shell of the
830 COO^- moiety are shown in green.

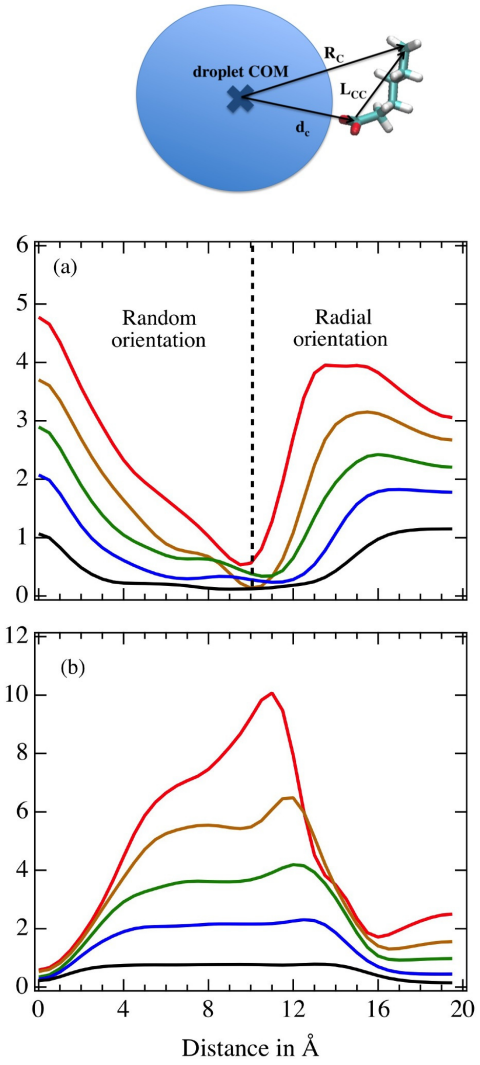

FIG. 6. Top: Definition of the geometric parameters R_C, d_c and L_{CC}. Middle and bottom: ΔR_C (a) and δR_C (b) quantities plotted as a function of d_c, for $N_w = 1000$ droplet systems. Black: ethanoate; blue: propanoate; green: butanoate; orange: pentanoate; red: hexanoate. The L_{CC} values in gas phase are 1.5, 3.3, 3.9 and 4.9 Å, from ethanoate to hexanoate, respectively.

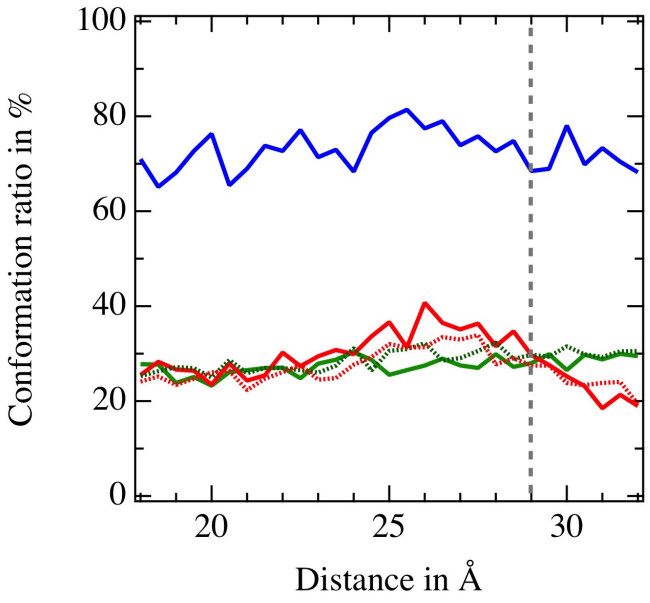

836

837 FIG. 7. Anti/gauche ratio for the conformations of the dihedral angles $\Psi_{n=4,5,6}$ for hexanoate (full
838 line) and $\Psi_{n=4,5}$ for pentanoate (dashed line), as a function of d_c, for air/liquid water interface
839 simulations. Red: Ψ_4; green: Ψ_5; blue: Ψ_6. The vertical dashed line indicates the position of the
840 air/liquid water interface.

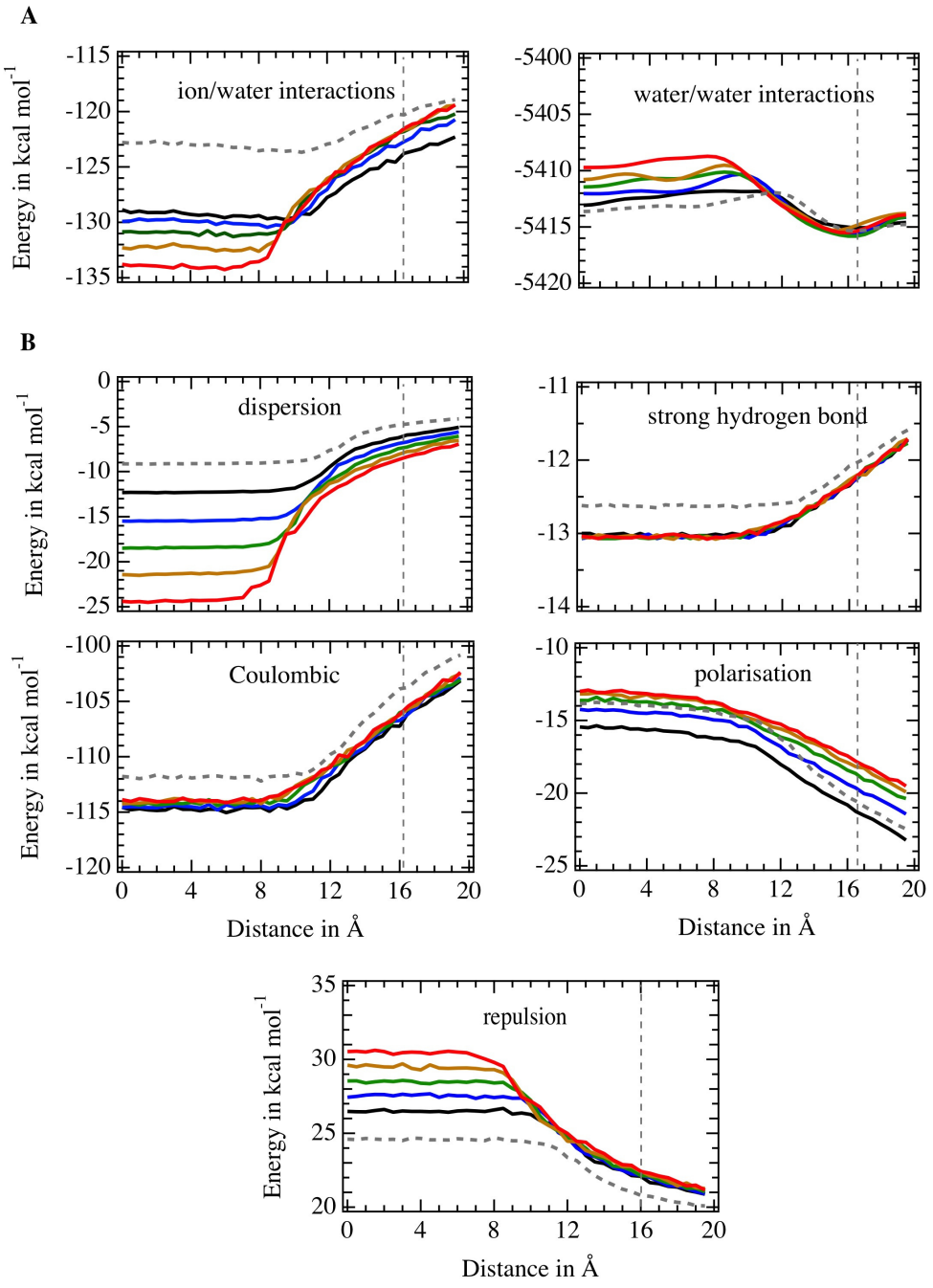

841

842 FIG. 8. **A**: Ion/water and water/water microscopic energies as a function of the ion location
843 for a $N_w = 600$ droplet. For water/water interactions, the original data are smoothed using a
844 binomial filter to reduce the noise due to evaporation effects. **B**: Components of the ion/water
845 interaction energies. Dashed grey line: $HCOO^-$; black line: CH_3COO^-; blue: $C_2H_5COO^-$; green:
846 $C_3H_7COO^-$; orange: $C_4H_9COO^-$; red: $C_5H_{11}COO^-$. The vertical dashed line indicates the
847 position of the droplet interface.

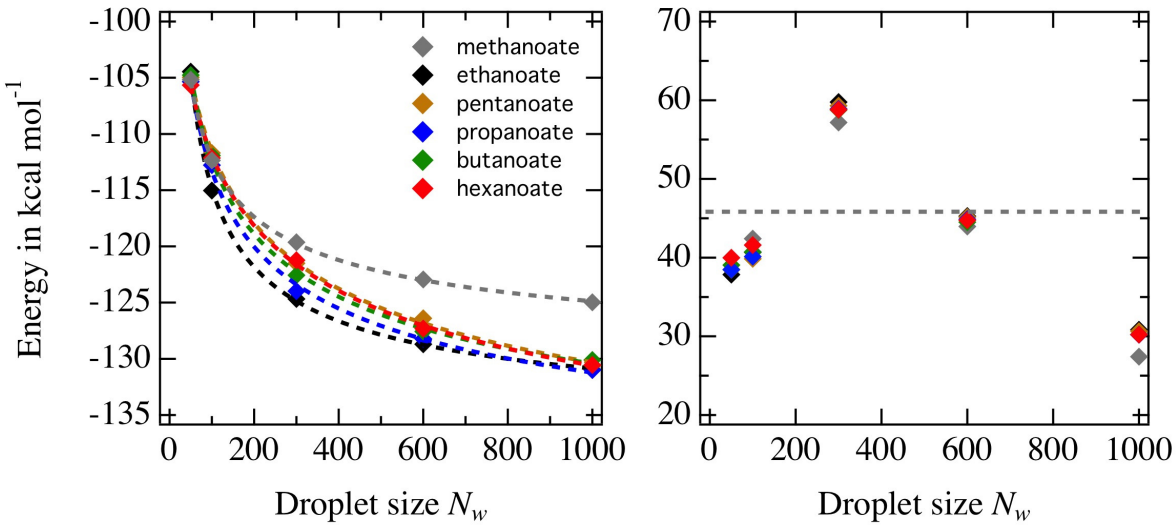

FIG. 9. Mean ion/water interaction (left) and water destabilization (right) energies as a function of the droplet size. For ion/water energies, the power-law fitting functions corresponding to $(a, \epsilon_1) different from (0, 0)$ are shown in dashed lines. For water destabilization energies, the horizontal dashed grey line corresponds to the mean bulk water destabilization energy. Compared to methylated ammonium ions, the droplet water destabilization energies appear to be closer in magnitude for all the carboxylates, however, they behave similarly, i.e., they reach a maximum for $N_w = 300$ and then they decrease well below the bulk values. Note that the uncertainty affecting the water destabilization energies due to evaporation phenomena is around $\pm$ 5 kcal mol^{-1}.

TABLES

Carboxylate	ΔH_g^{prot}	$\Delta H^{\mathrm{BH}}_{g\to aq}$	$\Delta H^0_{aq,\mathrm{dissociation}}$
$HCOO^-$	-345.3	-11.5	-0.04
CH_3COO^-	-348.5	-12.7	-0.10
$C_2H_5COO^-$	-347.5	-14.6	-0.14
$C_3H_7COO^-$	-346.5	-17.4	-0.69
$C_4H_9COO^-$	-346.2	-19.9	-0.70

TABLE I. Thermochemistry of carboxylate protonation and solvation. ΔH_g^{prot}: carboxylate protonation enthalpy in gas phase. $\Delta H^{\mathrm{BH}}_{g\to aq}$: absolute solvation enthalpy of a protonated carboxylate. $\Delta H^0_{aq,\mathrm{dissociation}}$: proton dissociation enthalpy in aqueous phase of a protonated carboxylate. All enthalpy data at room temperature and pressure, in kcal mol^{-1}, from Ref. 45.

	-$\Delta\bar{U}^{iw}(\infty)$				$\Delta\bar{U}_{\rm ww}$	$\Delta\bar{U}_{\rm intra}$	-$\Delta H_{g\to aq}$	$\Delta H_{g\to aq}(\mathrm{H^+})$
	(0,0)	(a,0)	(0,ϵ_1)	(a,ϵ_1)				
$HCOO^-$	136.0	133.6	133.3	133.6	46.4	0.0	87.7 (85.3)	269.1
CH_3COO^-	146.4	140.2	138.4	140.1	47.4	0.8	92.0 (89.7)	269.0
$C_2H_5COO^-$	145.7	147.3	147.3	145.0	46.4	0.3	100.5 (90.5)	261.7
$C_3H_7COO^-$	145.7	148.3	148.3	135.6	46.6	0.7	98.3 (92.9)	266.3
$C_4H_9COO^-$	143.7	155.7	151.7	155.6	46.5	1.0	107.4 (95.2)	259.4
$C_5H_{11}COO^-$	143.6	158.1	152.7	157.0	47.7	1.2	107.6 (-)	259.2
NH_4^+	122.2	124.4	124.1	124.4	35.3	0.0	89.0	273.0
$CH_3NH_3^+$	113.6	115.7	115.5	114.1	34.4	0.1	80.8	272.3
$(CH_3)_2NH_2^+$	106.4	104.9	104.8	102.4	33.4	0.3	70.3	269.0
$(CH_3)_3NH^+$	100.3	103.6	103.2	101.2	32.3	0.2	70.2	276.0
K^+	119.6	120.1	120.1	116.1	30.5	-	88.3	

TABLE II. Extrapolated ion/water energies $\Delta\bar{U}^{iw}(\infty)$, differences in ion intramolecular deformation energies $\Delta\bar{U}_{\rm intra}$ and in water destabilization energies $\Delta\bar{U}_{\rm ww}$ due to the presence of the ion in water, single ion solvation enthalpies $\Delta H_{g\to aq}$, and absolute proton solvation enthalpies $\Delta H_{g\to aq}(\mathrm{H^+})$. The four values for $\Delta\bar{U}^{iw}(\infty)$ correspond to the data extrapolated using different fitting functions, whose parameters a and/or ϵ_1 are set to zero or taken as adjustable. $\Delta H_{g\to aq}$ and $\Delta H_{g\to aq}(\mathrm{H^+})$ values are averaged from $\Delta\bar{U}^{iw}(\infty)$ values obtained with parameters different of (0,0). For $\Delta H_{g\to aq}$, the experimental values for carboxylates cited in parentheses are taken from Ref. [52]. All energy data in kcal mol^{-1}.